POLITECNICO DI TORINO
Repository ISTITUZIONALE

Convective heat transfer enhancement by diamond shaped micro-protruded patterns for heat sinks:
Thermal fluid dynamic investigation and novel optimization methodology

(Article begins on next page)

02 September 2025

Convective heat transfer enhancement by diamond shaped micro-protruded patterns for heat sinks: Thermal fluid dynamic investigation and novel optimization methodology

Luigi Ventola[a], Masoud Dialameh[a], Matteo Fasano[a], Eliodoro Chiavazzo[a], Pietro Asinari[a,*]

[a]*multi-Scale ModeLing Laboratory (SMaLL), Energy Department, Politecnico di Torino, Corso Duca degli Abruzzi 24, 10129 Torino, Italy*

Abstract

In the present work, micro-protruded patterns on flush mounted heat sinks for convective heat transfer enhancement are investigated and a novel methodology for thermal optimization is proposed. Patterned heat sinks are experimentally characterized in fully turbulent regime, and the role played by geometrical parameters and fluid dynamic scales are discussed. A methodology specifically suited for micro-protruded patterns optimization is designed, leading to 73 % enhancement in thermal performance respect to commercially available heat sinks, at fixed costs. This work is expected to introduce a new methodological approach for a more systematic and efficient development of solutions for electronics cooling.

Keywords: Optimization of processes, Convective heat transfer enhancement, Electronics cooling, Micro-protruded patterns, Design of

---

[*]corresponding author:
 Email address: `pietro.asinari@polito.it` (Pietro Asinari)

1. Introduction and motivations

The performance of electronic devices steadily grows with time according to the popular Moore's law, which states that the number of transistors in a dense integrated circuit doubles approximately every two years [1]. Consequently, heat fluxes to be dissipated in those devices progressively increase. The need for solutions able to deal with such high heat fluxes has motivated the investigation of a huge variety of methods and technologies for heat transfer enhancement [2]. Solutions based on liquid [3] and two-phase [4, 5] flows have been proved to be effective in dissipating large heat fluxes. Nevertheless, cooling strategies based on air are expected to remain a rather convenient and popular approach for a wide class of electronic devices (e.g. notebook computers, portable devices) in the next future, due to their low cost and reliability. However, the efficiency of these solutions needs to be continuously improved, in order to meet the increasing thermal requirements of next generation electronic devices [6, 7].

Novel solutions have been proposed, like innovative pin fin arrays with unusual [8] or non-uniform geometries [9], metal foams [10], dimpled surfaces [11, 12, 13], porous media [14], micro-protruded patterns [15, 16], artificial scale-roughness [17, 18] and carbon nanotube based structures [19]. In particular, heat sinks with either micro-protruded patterns or artificial scale-roughness show significant heat transfer augmentation [15, 18].

Recently, the authors of this work investigated several solutions based on both rough surfaces (manufactured by selective laser melting - SLM, also

2

known as direct metal laser sintering - DMLS [20, 21]), and on patterns of micro-structures (manufactured by laser-etching [22]) for enhancing convective heat transfer.

This work is focused on diamond shaped micro-protruded patterns, which are investigated as a promising method to enhance heat transfer performances of flush mounted heat sinks. More specifically, a systematic procedure based on design of experiments approach is proposed to:

- Investigate the convective heat transfer phenomenon, in order to understand, interpret and describe the effect of geometrical parameters and fluid dynamic scales on heat transfer;

- Design a novel methodology suitable for a reliable and automatic thermal optimization of micro-protruded patterns.

The paper is organized as follows. In Section 2, different diamond protruded patterns are rationally designed by taking advantage of the design of experiments approach. In Section 3, the experimental setup used to test the diamond protruded patterns is described. In Section 4, the results of experimental characterization are reported and a mathematical model describing the influence of geometrical parameters and flow regimes on thermal transmittance of diamond protruded patterns is developed. In Section 5, the thermal fluid dynamics features of diamond micro-protruded patterns for heat sinks are discussed, and a novel optimization methodology proposed. Finally, in Section 6, conclusions and perspectives are reported.

3

2. Design of experiments

To obtain an independent benchmark of data, nine copper samples, each characterized by a peculiar Diamond micro-Protruded Pattern (DPP), are designed and manufactured by milling. The convective heat transfer coefficient for each sample is measured. The bottom part of each sample consists in a parallelepiped block (11.1 x 11.1 x 5 mm^3), which can be mounted in the experimental test bench described in Section 3. Samples are characterized by diamond micro-protrusions, which are arranged in a regular pattern. Each diamond shaped micro-protrusion is a parallelepiped pin, with a d x d square section rotated by 45 degrees with respect to the main flow direction. Protrusions are arranged according to a staggered configuration, as represented in Fig. 1.

A DPP is fully determined by 3 geometrical independent degrees of freedom (DoF). There are no constrains in choosing the DoF to use for the design, except for their property of independence. As an example, given the height of the protrusion H, the base edge of the protrusion d, the pitch between neighboring protrusions p (see Fig. 1), the number of protrusions N and $s = p - d$, a possible choice for the 3 DoF could be $\{H, p, d\}$. However, the use of dimensionless parameters is preferable, as they typically ensure a wider generality of results.

In previous studies on heat transfer through protruded patterns, the ratios between characteristic geometrical lengths have been adopted as governing parameters for the measured thermal performances. For example, Garimella *et al.* [24] chose the ratios between (i) spacing and protrusions height and (ii) channel height and protrusions height as significant parameters for charac-
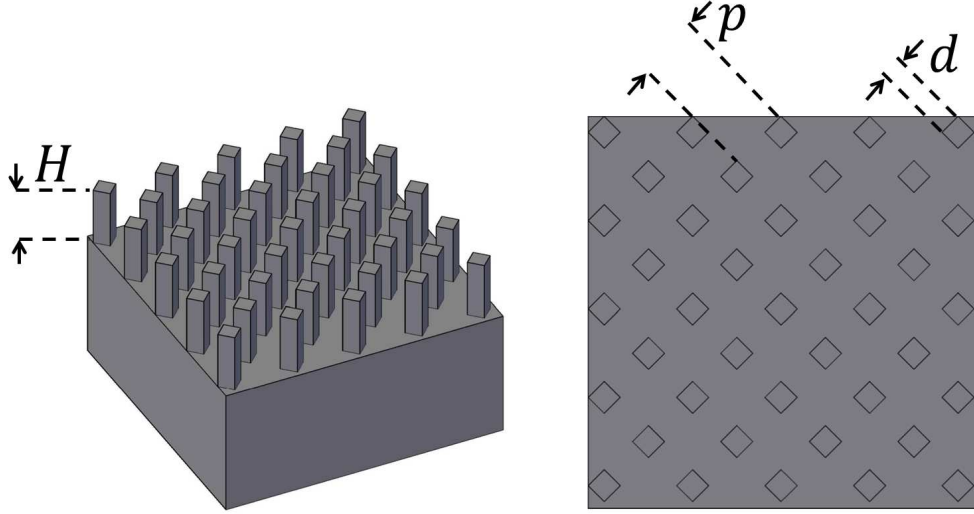
Figure 1: Sample geometry: Isometric view (left-hand side) and top view (right-hand side).

terizing heat transfer phenomenon in arrays of protruding elements. Leung *et al* [25], instead, chose the ratio between base length and height of protrusions, as well as the ratio between channel height and protrusions height as characterizing parameters.

In this work, to design our test matrix, a novel set of geometrical dimensionless parameters is considered. The investigation of those specific parameters is proved to be suitable in developing a novel methodology for the thermal optimization of micro-protruded patterns for heat sinks. In this context, we consider as optimal configuration the one ensuring the maximum thermal transmittance, at fixed amount of material needed to manufacture the micro-protrusions. In fact, the amount of used material is a suitable production cost indicator for most of the "not subtractive" manufacturing

technologies, both traditional (e.g. extrusion) and innovative (e.g. additive manufacturing, SLM) ones. In other words, optimal configuration is intended to be the one that guarantees the maximum thermal performance per unit of production costs. Parameters investigated in this study are:

- Plane solidity (or plan area density) λ_p, defined as the fraction of the root surface area (i.e. in our case $A_n = 11.1^2 \ mm^2 = 123 \ mm^2$) covered by protrusions (see Fig. 1, top view). This parameter expresses the pattern density, and it ranges from 0 to 1; Low values of λ_p refer to sparse patterns, whilst high values denote dense patterns (see also Fig. 2 in ref. [26]).

- Enhancement ratio in convective heat transfer surface area A/A_n, where A is the sample area, which is defined as the sum of root surface area and protrusions surface area, namely $A = A_n + 4dHN$.

- Dimensionless mixed length $V/(AY_0)$, where $V = NHd^2$ is the volume of the micro-protrusions and $Y_0 = 0.0503 \ mm$ is the average viscous length (or average wall unit [27]), which is calculated as the mean viscous length over the range of fluid flows (i.e. Reynolds numbers) investigated in this study. The dimensionless mixed length is obtained as a ratio between geometric (V/A) and fluid dynamic (Y_0) lengths. In particular, V/A represents the ratio between the amount of material for manufacturing the protrusions (i.e. production cost indicator) and the available surface area involved in the heat transfer phenomenon, while Y_0 is strictly related to the boundary layer thickness.

Comparing geometric and fluid dynamics scales is essential to understand

their interactions, as well as to determine how the optimal geometrical DPP configuration depends on the flow field. It is worth to mention that $V/(AY_0)$ is not the only mixed length analyzed in this study. In the following, the importance of the dimensionless protrusion height H/Y_0 is also discussed. This parameter represents the ratio between protrusion height and boundary layer thickness, and it quantifies the penetration of protrusions into the boundary layer. In the following, we refer to the three parameters defined above as *model* parameters, because they are expected to significantly affect both the thermal transmittance of the heat sink Tr $[W/K]$ and the volume of the micro-protruded pattern, therefore allowing to define an optimization criteria. λ_p plays a key role on the interactions between thermal fluid dynamics structures (i.e. eddies, boundary layers, etc.) and micro-structures, thus strongly affecting the convective heat transfer coefficient h $[W/m^2/K]$. For instance, λ_p is often used to study the interactions between buildings and the atmospheric boundary layer [26] , but it has been demonstrated to be very effective in describing interactions between fluid dynamics structures and micro-structures in a macroscopic channel too [21]. The A/A_n parameter is considered because heat flux, thus Tr, is strongly affected by the surface area involved in the heat transfer phenomenon. Since these two parameters are not directly linked to the production cost parameter (V), a third parameter $V/(AY_0)$ is also included.

The three model parameter described above can be expressed as function of the geometrical parameters $\{H, p, d\}$ as:

$$\lambda_p = \frac{Nd^2}{A_n} = \frac{d^2}{p^2},$$

(1)

$$\frac{A}{A_n} = \frac{4dH}{p^2} + 1, \tag{2}$$

$$\frac{V}{AY_0} = \frac{Hd^2}{Y_0(4dH + p^2)}. \tag{3}$$

These equations are valid under the assumption that the number of protrusions N can be expressed as:

$$N = \frac{A_n}{p^2}. \tag{4}$$

Obviously, the model parameters have a physical meaning only if:

$$\begin{cases} 0 < \lambda_p < 1, \\ A/A_n > 1, \\ V/(AY_0) > 0. \end{cases} \tag{5}$$

Any existing DPP is fully determined by defining all components of the vector $\left\{\lambda_p, \frac{A}{A_n}, \frac{V}{AY_0}\right\}$. In this study the tested DPPs are designed taking advantage of the Design Of Experiments (DOE) approach. In particular, a Taguchi (or L9 orthogonal arrays) based, 3 levels-3 factors, fractional DOE is applied [28]. Each parameter (or factor) can assume three possible values (or levels), namely low (1), medium (2) or high (3), as listed in Table 1. Therefore, once the levels per each parameters have been defined, the geometry of the nine DPPs to be tested is determined according to the test matrix proposed in ref. [28] and reported in Table 2.

Due to the rough tolerances of the milling process, the actual parameters of the samples are slightly different from the design values reported in Table 1: in Table 3, the model parameters and the extra geometrical quantities are reported for each sample. Fig. 2 shows how all samples are located in

Table 1: Design values and associated levels for each model parameter.

parameter level	λ_p	A/A_n	$V/(AY_0)$
1	0.15	1.5	2
2	0.35	2.5	2.75
3	0.55	3.5	3.5

the parameter space; whereas Fig. 3 reports the pictures of the analyzed samples.

It is worth to provide more details on the calculation of Y_0. The average viscous length Y_0 can be defined as:

$$Y_0 = \frac{1}{Re_{D,max} - Re_{D,min}} \int_{Re_{D,min}}^{Re_{D,max}} y_0(Re_D) \, dRe_D \quad . \tag{6}$$

As demonstrated in [21], in case of smooth pipe turbulent flow, viscous length y_0 depends on the hydraulic diameter based Reynolds number $Re_D = uD/\nu$ as:

$$y_0 = \frac{D}{Re_D \sqrt{f_B/8}}, \tag{7}$$

where $f_B = f_B(Re_D) = 0.3164 \, Re_D^{-1/4}$ is the friction factor expressed by the phenomenological correlation proposed by Blasius [29], u is the average fluid velocity, D is the hydraulic diameter, and ν is the fluid kinematic viscosity.

Table 2: Test matrix [28].

sample	λ_p level	A/A_n level	$V/(AY_0)$ level
#1	1	1	1
#2	1	2	2
#3	1	3	3
#4	2	1	2
#5	2	2	3
#6	3	3	2
#7	3	1	3
#8	3	2	1
#9	2	3	1

Table 3: Values of model parameters and extra geometrical quantities for the tested samples.

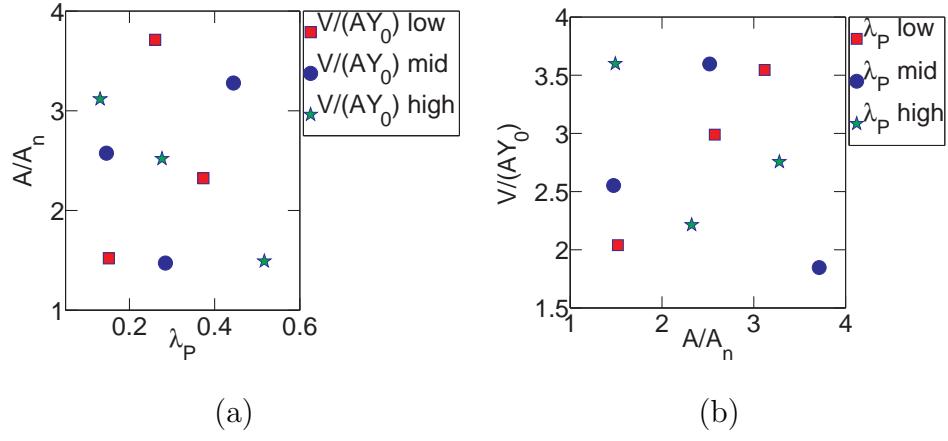| Sample	λ_p	A/A_n	$V/(AY_0)$	H [mm]	d [mm]	p [mm]	s [mm]
#1	0.15	1.52	2.04	1.03	1.20	3.08	1.88
#2	0.15	2.57	2.99	2.45	1.00	2.62	1.62
#3	0.13	3.12	3.55	4.78	1.05	2.90	1.85
#4	0.28	1.47	2.55	0.70	1.60	3.00	1.40
#5	0.28	2.52	3.60	1.56	1.20	2.28	1.08
#6	0.44	3.28	2.76	1.05	0.80	1.20	0.40
#7	0.52	1.49	3.60	0.55	2.30	3.20	0.90
#8	0.37	2.32	2.21	0.56	0.67	1.10	0.43
#9	0.26	3.71	1.85	1.16	0.52	1.02	0.50

Figure 2: Collocation of samples in the model parameter space. Due to manufacturing tolerances, a non uniform sampling of the parameter space is considered.
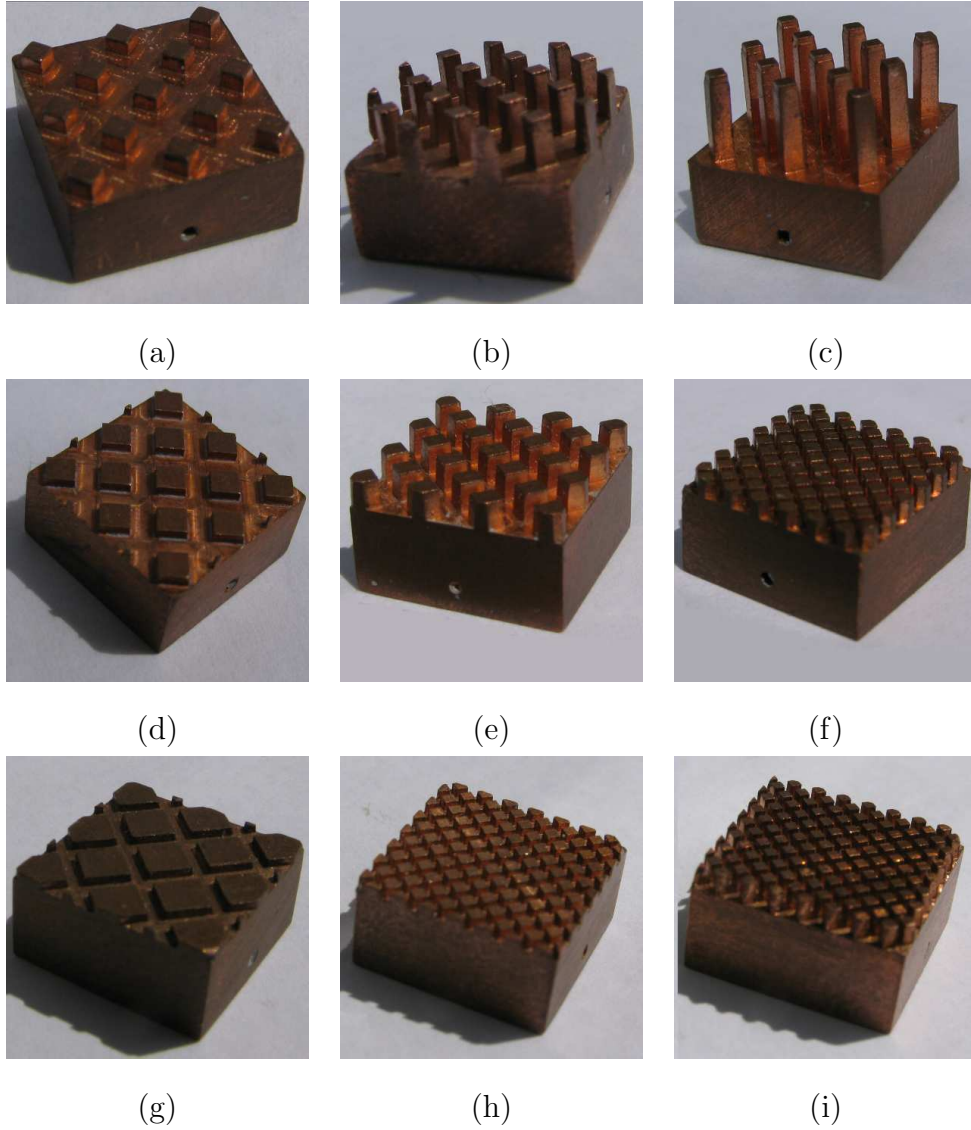
(a)　　　　　　　(b)　　　　　　　(c)

(d)　　　　　　　(e)　　　　　　　(f)

(g)　　　　　　　(h)　　　　　　　(i)

Figure 3: Tested samples.

3. Experimental setup

An open loop wind tunnel with cross section of $228\,mm \times 158\,mm$ is used to control the flow field. An anemometer is used to measure the air velocity

u_{ax} at the axis of the wind tunnel (see Fig. 4). A developed sensor (described in detail in [23]) is used to measure the convective heat transfer coefficient. This sensor is based on the key idea of thermal guard. An electrical heater at the bottom of the sample generates a controlled heat flux. The sample is surrounded by a temperature controlled "guard" made of copper, which is kept at the same temperature of the sample, thus forcing the heat to flow into the sample only. Temperatures are monitored by thermocouples inserted in the sample, in the upstream and downstream (referring to fluid flow) walls of the guard. Nevertheless, some parasite conductive heat fluxes between the sample and the guard could possibly arise. In order to significantly reduce those undesired fluxes, a thermal insulating shield made of Teflon™ is placed between sample and guard. In Fig. 5 a cross-sectional sketch of the sensor is reported. The experimental procedure used to characterize the samples has been refined and detailed in previous works [23].
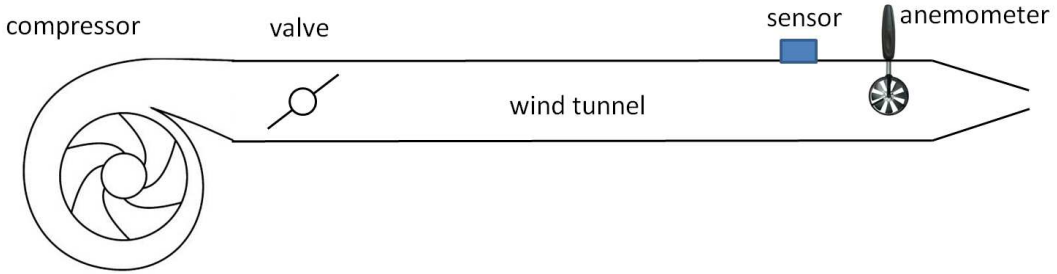

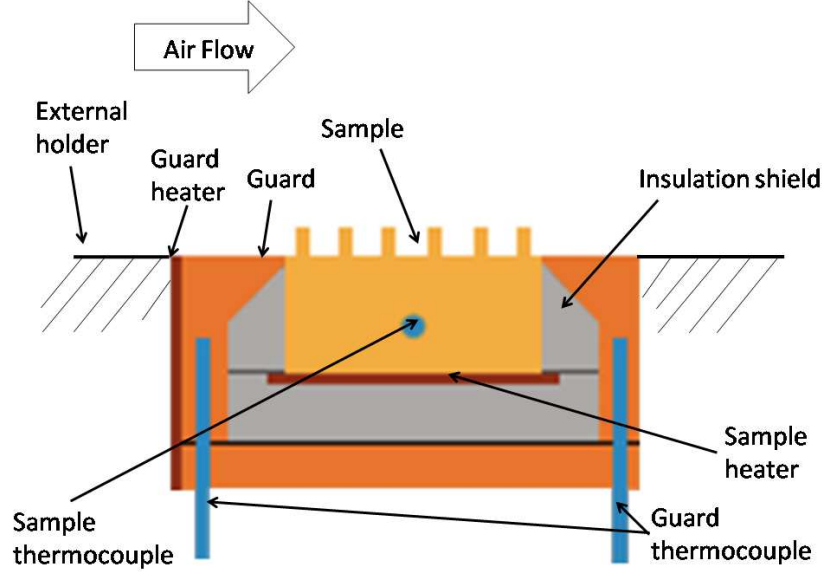Figure 4: Schematics of the experimental test bench.

Figure 5: Cross-sectional sketch of the convective heat transfer sensor (see ref. [23]).

4. Experimental characterization and data reduction

In this section, the experimental thermal characterization of all samples is provided. Moreover, the experimental results are compared to the model obtained by data reduction analysis.

The measured velocity u_{ax} is used to calculate the Reynolds number $Re_D^{ax} = u_{ax}D/\nu$. Nevertheless, experimental data for pipe and duct flows are often reported in terms of average velocity based Reynolds number Re_D. The relation between these two different Reynolds numbers can be expressed as $Re_D = 0.694\ (Re_D^{ax})^{1.0162}$, as demonstrated elsewhere [23]. In particular, for flush mounted heat sinks the use of heated edge instead of the hydraulic diameter as characteristic length scale has been proved to be more effective

14

[30, 31]. Consequently, Heat transfer performance of each sample is reported as function of the heated edge, average velocity based Reynolds number: $Re_L = uL/\nu$, where $\nu = 1.544 \times 10^{-5} \ m^2/s$, and $L = 20 \ mm$ is the heated edge, namely the guard edge. In order to make the results more general and easier to be compared with other studies and benchmarks, the relation between Re_L and $Re_L^{ax} = u_{ax}L/\nu$ (i.e. the heated edge, axial velocity based Reynolds number) is reported: $Re_L = 0.669 \ (Re_L^{ax})^{1.0162}$.

In Fig. 6, the convective heat transfer coefficient of all samples is reported in terms of $Nu_L/Pr^{0.33}$, where $Nu_L = hL/\lambda$ is the dimensionless Nusselt number, and $Pr = \nu/\alpha$ is the dimensionless Prandtl number, being $\lambda = 2.622 \times 10^{-2} \ W/m/K$ and $\alpha = 2.224 \times 10^{-5} \ m^2/s$ air thermal conductivity and thermal diffusivity, respectively. In Fig. 7, thermal transmittances $Tr = hA$ of samples are shown. In both Fig. 6 and Fig. 7, the experimental characterization of a reference flat sample (i.e. without protrusion) is reported. The model is obtained by data reduction analysis discussed in the following. Finally, in Fig. 8, the results in terms of quantity Tr/V are reported. Error bars reported in Figs. 6, 7, 8 are estimated according to the methodology discussed in [21]. In particular, we perform both type A and type B evaluation of uncertainties, and we adopt a significance level $\alpha = 0.05$ (5%).

In the following, we propose a model able to predict the convective thermal transmittance of a generic DPP heat sink as a function of model parameters $\left\{ \lambda_p, \frac{A}{A_n}, \frac{V}{AY_0} \right\}$ and fluid flow regime, namely Re_L. The model is based on data reduction on the experimental measurements of Tr. A reference Reynolds number is defined:
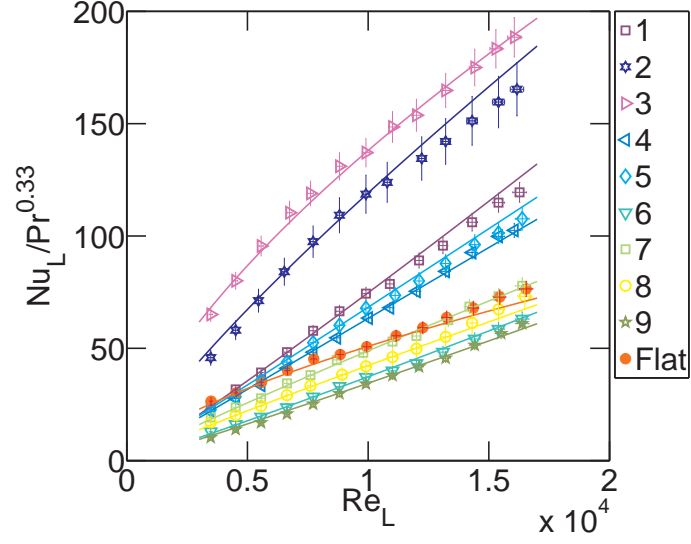
Figure 6: Comparison between experimental (symbols) and model (solid lines) results in terms of $Nu_L/Pr^{0.33}$.
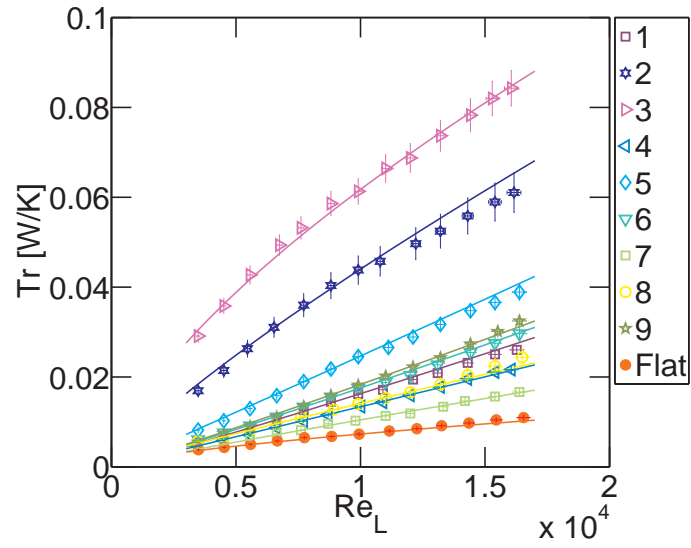

Figure 7: Comparison between experimental (symbols) and model (solid lines) results in terms of Tr.
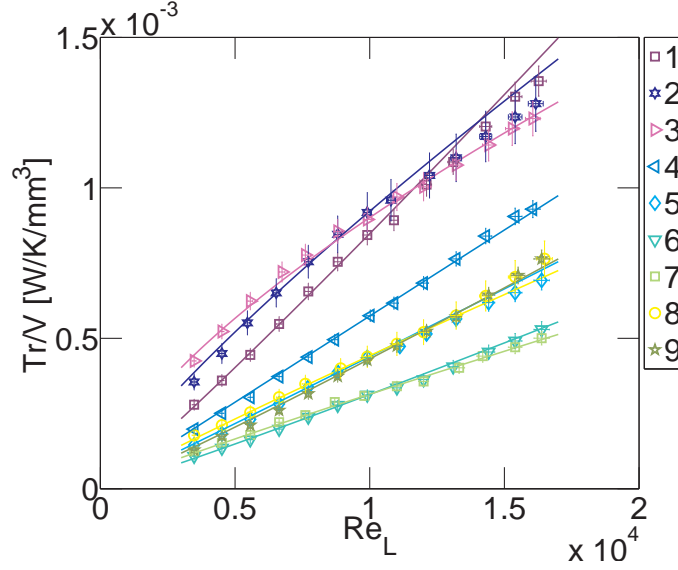
16

Figure 8: Comparison between experimental (symbols) and model (solid lines) results in terms of Tr/V.

$$Re_{L,R} = 10^4, \tag{8}$$

while Tr is modeled as the product of two functions:

$$Tr = gTr_R. \tag{9}$$

In Eq. 9, Tr_R is the transmittance value at the reference Reynolds number, which is expected to depend on the model parameters $\left\{\lambda_p, \frac{A}{A_n}, \frac{V}{AY_0}\right\}$. On the other hand, g accounts for thermal transmittance as we move away from the reference flow regime, and it is modeled as a function of $\frac{H}{Y_0} = \frac{H}{Y_0}\left(\lambda_p, \frac{A}{A_n}, \frac{V}{AY_0}\right)$ and Reynolds number ratio $Re_L/Re_{L,R}$.

The quantity Tr_R can be split into $Tr_R = Tr_R^0 + \Delta Tr_R$, where Tr_R^0 is the transmittance of flat surface at the reference Reynolds number, while ΔTr_R

17

is the additional transmittance due to the presence of DPP on the heat sink. Consequently, Tr_R can be modeled as:

$$Tr_R = Tr_R^0 + V\frac{\Delta Tr_R}{V}. \tag{10}$$

In this form, V represents the amount of additional raw material needed to manufacture the protruded pattern, while the parameter $\frac{\Delta Tr_R}{V}$ represents the enhancement in thermal transmittance of the device achieved per unit volume. $\frac{\Delta Tr_R}{V}$ is modeled by a second order polynomial function as:

$$
\begin{aligned}
\frac{\Delta Tr_R}{V} &= c_1\widehat{\lambda_p} + c_2\frac{\widehat{A}}{A_n} + c_3\frac{\widehat{V}}{AY_0} + c_4\widehat{\lambda_p}^2 + c_5\frac{\widehat{A}}{A_n}^2 + c_6\frac{\widehat{V}}{AY_0}^2 \\
&\quad + c_7\widehat{\lambda_p}\frac{\widehat{A}}{A_n} + c_8\widehat{\lambda_p}\frac{\widehat{V}}{AY_0} + c_9\frac{\widehat{A}}{A_n}\frac{\widehat{V}}{AY_0}.
\end{aligned} \tag{11}
$$

where the superscript $\widehat{}$ indicates the *normalized* model parameters, obtained as:

$$
\begin{cases}
\widehat{\lambda_p} = \frac{\lambda_p}{(\lambda_p)_{Avr}}, & (\lambda_p)_{Avr} = \frac{1}{9}\sum_{i=1}^{9}(\lambda_p)_i \\[3mm]
\frac{\widehat{A}}{A_n} = \frac{\frac{A}{A_n}}{\left(\frac{A}{A_n}\right)_{Avr}}, & \left(\frac{A}{A_n}\right)_{Avr} = \frac{1}{9}\sum_{i=1}^{9}\left(\frac{A}{A_n}\right)_i \\[3mm]
\frac{\widehat{V}}{AY_0} = \frac{\frac{V}{AY_0}}{\left(\frac{V}{AY_0}\right)_{Avr}}, & \left(\frac{V}{AY_0}\right)_{Avr} = \frac{1}{9}\sum_{i=1}^{9}\left(\frac{V}{AY_0}\right)_i
\end{cases} \tag{12}
$$

Subscript i in equation above denotes the i-th sample.

The vector $\{C\} = \{c_1, c_2, c_3, c_4, c_5, c_6, c_7, c_8, c_9\}$ collects all the model coefficients, which are obtained by a regression procedure from the experimental data (see Appendix A for further details). In particular, from the data regression, we obtain $c_1 = -0.0003$, $c_2 = +0.0010$, $c_3 = -0.0003$,

$c_4 = -0.0013$, $c_5 = -0.0011$, $c_6 = -0.0073$, $c_7 = -0.0041$, $c_8 = +0.0067$, $c_9 = +0.0076$.

The function $g = \frac{Tr}{Tr_R}$ is modeled as:

$$g = \left(\frac{Re_L}{Re_{L,R}} \right)^B = \left(\frac{Re_L}{10^4} \right)^B , \tag{13}$$

where $B = B\left(\frac{H}{Y_0}\right)$ is computed as:

$$B = \log_{\frac{Re_L}{10^4}} \frac{Tr}{Tr_R}. \tag{14}$$

From the tested samples, ten experimental values of B are available for data regression. Considering a least mean squares fitting procedure, results are best fitted by:

$$B = d_1 \left(\frac{H}{Y_0} \right)^{d_2} exp \left(-d_3 \frac{H}{Y_0} \right) + d_4, \tag{15}$$

where the fitting parameters d_1, d_2, d_3, d_4 assume the values 0.003316, 2.3, 0.1039 and 0.66, respectively. In Fig. 9, the comparison between experimental values of B and the corresponding analytical model described by Eq. 15 is shown.

It is worth of note that the proposed model reveals an excellent agreement with experimental data, as shown in Figs. 6, 7, 8. Modeling Tr by mean of the variable separation approach (Eq. 9) allows to independently quantify the effects of the geometrical parameters $\left\{ \lambda_p, \frac{A}{A_n}, \frac{V}{AY_0} \right\}$ and of the fluid dynamic parameter Re_L, respectively. Concerning Tr_R, the original strategy of applying data reduction procedure to the quantity $\Delta Tr/V$ makes the model very appropriate for its implementation in the optimization procedure for micro-structured patterns discussed in Section 5.2, i.e. where the

goal is to maximize the latter quantity. Moreover, the chosen geometry variables for Tr_R are proved to be very effective in determining convective heat transfer on DPP. In particular, λ_p is very important, as discussed in Section 5.1. Concerning the g function, it sheds light on the crucial role of H/Y_0 in determining how the fluid flow regime, i.e. Re_L, influences the thermal transmittance, and on the existence of an optimal value of H/Y_0 (See Fig. 9), discussed in Section 5.1. Those insights on micro patterned surfaces are novel, to our knowledge. As a conclusion, the proposed model is a very effective tool for a fast design of micro-patterned heat sinks. To the best of our knowledge, a similar tool was never been proposed in literature so far.
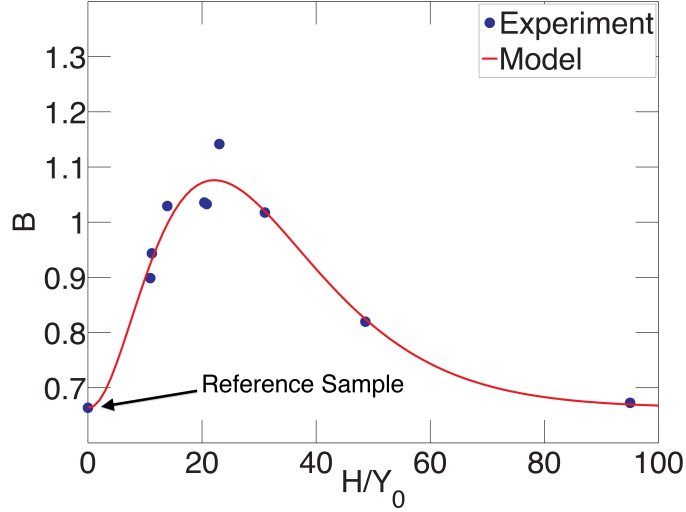

Figure 9: Comparison between experimental values of B and the best fitted analytical model.

Finally, we define some quantities useful to discuss the presented results. Firstly, we introduce dimensionless fin parameter ml, where l is the protru-

sion height H defined in Table 3, and m is defined as [32]:

$$m = \left(\frac{4h}{\lambda_{Cu}d}\right)^{0.5},$$ (16)

where $\lambda_{Cu} = 388 \ W/m/K$ is the thermal conductivity of copper. Secondly, we introduce the aerothermal efficiency η_A, defined as [33]:

$$\eta_A = \frac{Nu_L/Nu_L^0}{(f/f^0)^{1/3}},$$ (17)

where Nu_L^0 and f^0 are Nusselt number and friction factor referred to a reference condition (e.g. flat sample), respectively.

5. Results and optimization methodology

5.1. thermal fluid dynamics features of diamond micro-protruded patterns for heat sinks

In the following, the experimental results presented in Section 4 are interpreted, and the main thermal fluid dynamic features of diamond micro-protruded patterns discussed.

Before proceeding further, it is worth of note that the fin efficiency plays negligible role in convective heat transfer of the considered diamond micro-protruded patterns. In fact, here the temperature gradient along the protrusions length is very small. To prove this, for each protrusion we calculate ml by Eq. 16 considering $h = h_{max} = 200 \ W/m^2/K$, i.e. the maximum convective heat transfer coefficient experimentally measured. As a result, the fin efficiency is higher than 98 % in all the considered samples, hence its effect is negligible.

The parameter λ_p plays a key role in controlling the condition of fluid stagnation and, consequently, the convective heat transfer coefficient. As shown in Fig. 6, samples characterized by low λ_p (i.e. #1, #2 and #3) experience larger values of $Nu_L/Pr^{0.33}$ than samples with higher λ_p (i.e. #6, #7, #8 and #9). Focusing on sparse patterns (low λ_p) it can be noticed that H significantly influences $Nu_L/Pr^{0.33}$, which monotonically increases with H. This is due to the fact that higher protrusions are able to penetrate deeper in the fluid boundary layer, hence they are flushed by stronger flow field (see Fig. 6). This phenomenon allows to achieve a huge increase in convective heat transfer: the sample with the highest protrusions (sample #3) experiences an enhancement in $Nu_L/Pr^{0.33}$, almost constant over the entire range of Re_L under study, up to 150 % as compared to flat surfaces, while Tr increases up to 700 %. On the other hand, by increasing the density of patterns (i.e. increasing λ_p), fluid stagnation takes place and consequently $Nu_L/Pr^{0.33}$ decreases. In particular, very high density patterns, can experience values of $Nu_L/Pr^{0.33}$ even lower than flat surface (see sample #6, #7, #8 and #9). In Fig. 10, the influence of λ_p on $Nu_L/Pr^{0.33}$ is shown. Here, a comparison of nine experimental points with an exponential-based fitting curve is reported. This clearly demonstrates that λ_p plays a significant role: $Nu_L/Pr^{0.33}$ monotonically decreases with increasing λ_p, even though this result is limited to the range of λ_p considered in this work.
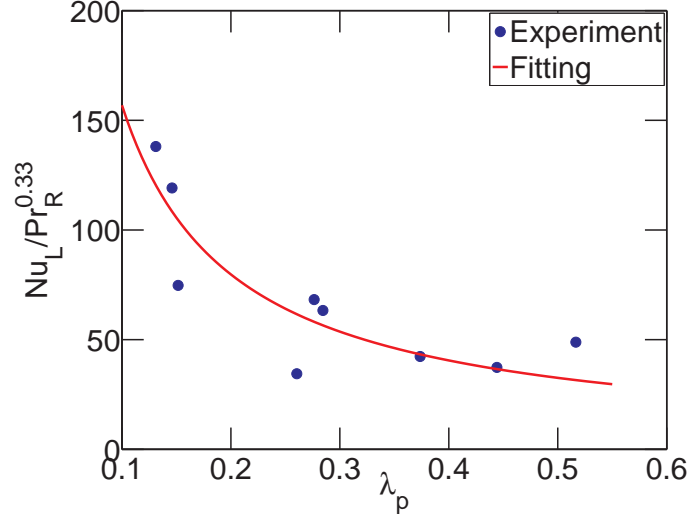
Figure 10: Influence of λ_p on $Nu_L/Pr^{0.33}$.

In all the tested samples, H/Y_0 plays a key role in determining how the fluid flow regime, i.e. Re_L, influences the thermal transmittance. In particular, Fig. 9 suggests that an optimal value of H/Y_0 exists, which lies in the range $10 < H/y_0 < 40$, where protrusions are at least twice the viscous sub-layer height ($\approx 5\ y_0$ according [27]), but still short enough to remain in the viscous wall region ($\leq 50\ y_0$ according [27]). Being y_0 inversely proportional to the Reynolds number (according Eq. 7) the optimal height H is expected to be function (monotonically decreasing) of the Reynolds number too. This is confirmed by experimental results: Being $\frac{Tr}{V}$ the parameter to maximize, and focusing on the three samples characterized by the lowest values of λ_p (hence the highest convective heat transfer coefficient), we can notice in Fig. 8 that in the low Reynolds number range ($0.3 \times 10^4 < Re_L < 0.9 \times 10^4$) the sample #3 (with the highest value of H), experiences the

highest $\frac{Tr}{V}$. In the intermediate Reynolds number range ($0.9 \times 10^4 < Re_L < 1.4 \times 10^4$), the sample #2 (with the intermediate H, among the three ones) experiences the highest $\frac{Tr}{V}$. Finally, in the high Reynolds number range ($1.4 \times 10^4 < Re_L < 1.7 \times 10^4$), the sample #1 (with the lowest H) experiences the highest $\frac{Tr}{V}$. Consequently, The optimal configuration depends on Re_L.

This evidence, emerged from the experimental results, is discussed in the following to provide general guidelines for a proper design of micro-structured patterns. Firstly, results prove an enhancement in convective heat transfer is achieved only for sparse patterns. Consequently, we suggest to choose a value of λ_p around 0.15 and not exceeding 0.33, because all tested patterns with $\lambda_p > 0.33$ are characterized by a heat transfer coefficient lower than the flat case (i.e. no protrusions). Secondly, the choice of H depends on the design target: results reveal that, for a given (low) value of λ_p, the higher H the higher the heat transfer coefficient. Nevertheless, a careful analysis of the results also recommends a choice of H/y_0 around 30 to maximize Tr/V. Hence, high values of H (but still short enough to guarantee high fin efficiency) are desirable for applications where high heat transfer coefficients are required. On the contrary, a value around 30 for H/y_0 is recommended when the goal of the design is use the minimum amount of material.

5.2. Optimization methodology of diamond micro-protruded patterns for heat sinks

In this section, an automatic methodology for *thermal optimization* of diamond micro-protruded patterns for heat sinks is presented. In addition, the algorithm is implemented and applied to a real case study and results are reported and discussed.

Input parameters of the algorithm are the heat sink working conditions, namely Reynolds number $Re_{L,W}$, heat flux to be removed Q_W and the temperature difference between heat sink and cooling fluid ΔT_W. As a result, the automatic optimization algorithm provides geometrical configurations, (in terms of $\left\{\lambda_p, \frac{A}{A_n}, \frac{V}{AY_0}\right\}$ or equivalently $\{H, d, p\}$) that maximize $\frac{Tr_W}{V}$ (namely the thermal transmittance per unit of production cost), while guarantee $Tr = Tr_W = \frac{Q_W}{\Delta T_W}$.

The proposed algorithm considers all the possible configurations, i.e. parameter combinations $\left\{\lambda_p, \frac{A}{A_n}, \frac{V}{AY_0}\right\}$, within the parameter range investigated by experiments (where data regression is proved to be valid). For each configuration, the algorithm calculates the corresponding values of V and Tr through the model provided by data regression (Eq. 9). Among all the possible configurations, the algorithm retains the ones that guarantee $Tr = Tr_W$ and discard the others. Finally, among the retained configurations, the one characterized by the minimum value of V is chosen. In particular, the parameter space (i.e. the possible DPP configurations) is numerically explored as follows: Each parameter can assumes 20 possible discrete values, by uniformly partitioning the parameter range. Then, the algorithm calculates the value of Tr associated to each of the $20^3 = 8000$ possible DPP configurations (i.e. possible combination of the 3 model parameters). Tr_W is compared to the value of Tr for each configuration, and configurations that match Tr_W with a tolerance of 5% are retained.

We notice that optimization of heat transfer devices typically includes both thermal transmittances and pressure losses, hence optimization problems usually deal with efficiency parameters that consider both the afore-

mentioned phenomena, e.g. η_A defined by Eq. 17. In this work, we neglect the effects of protruded patterns on pressure losses, because this study is focused on applications where these effects are not significant (e.g. power electronics for control of HVAC system in cars). Nevertheless, we stress that the methodology presented in this work could be extended to a more general case, by simply substituting $\frac{Tr_W}{V}$ (thermal performances per unit of production cost) with η_A as the parameter to be maximized. In such a way, the proposed optimization methodology find the DPP configuration able to minimize the pressure drop due to the heat sink, and consequently to maximize the thermal transmittance per unit of operating costs.

As a real case study, the developed algorithm is used to perform thermal optimization of DPP heat sink, i.e. maximum transmittance per unit of production costs, for three different Reynolds numbers, namely $Re_L = 0.5 \times 10^4, 10^4$ and 1.5×10^4, and with a range of transmittance values: $0.02 < Tr_W < 0.1 \ W/K$. In Tables 4, 5, and 6 the optimal geometrical parameters of DPP heat sinks for different Tr are reported, in the case of $Re_L = 0.5 \times 10^4, 10^4$ and 1.5×10^4, respectively. It is worth of note that for $Re_L = 0.5 \times 10^4$ the maximum transmittance is $Tr = 0.045 \ W/K$, because the parameter space explored in the optimization process is limited to the one investigated by experiments. Fig. 11 summarizes results of that case study: on the abscissa is reported DPP volume V, namely the production cost index, while on the ordinate the maximum (hence optimal) thermal transmittance Tr_{max} achieved for the three Reynolds numbers under exam is shown. It can be noticed that the volume, and consequently the production cost of the device, increases by decreasing Re_L (worst convective heat transfer).

In Table 7 optimal designs obtained by imposing $Tr_W = 0.03 \ W/K$ for the three different Re_L are compared. It is worth of note that optimal values of H chosen by our optimization algorithm are such that the corresponding ratio H/y_0 lies in the range $30 \div 35$. This result strengthen the hypothesis, exposed in Section 5.1, of the existence of an optimal value of H/y_0 lying in the range $10 < H/y_0 < 40$.

Finally, it is interesting to compare the configurations obtained from the optimization algorithm with the nine tested samples. Focusing on reference flow conditions $(Re_{L,R} = 10^4)$, Fig. 8 shows that sample #2 has the best value of transmittance per production costs unit (i.e. highest Tr/V) among the tested samples, being characterized by $Tr = 0.044 \ W/K$ and $V = 47.7$ mm^3. Instead, As shown in Fig. 11 and Tab. 5, the optimal configuration found by the algorithm allows to achieve $Tr = 0.092$ with the same amount of material, i.e. at fixed production costs. Therefore, this example shows that the presented thermal optimization procedure would allow to achieve a 110 % enhancement in the thermal transmittance of the best performing tested sample, while keeping production costs unchanged.
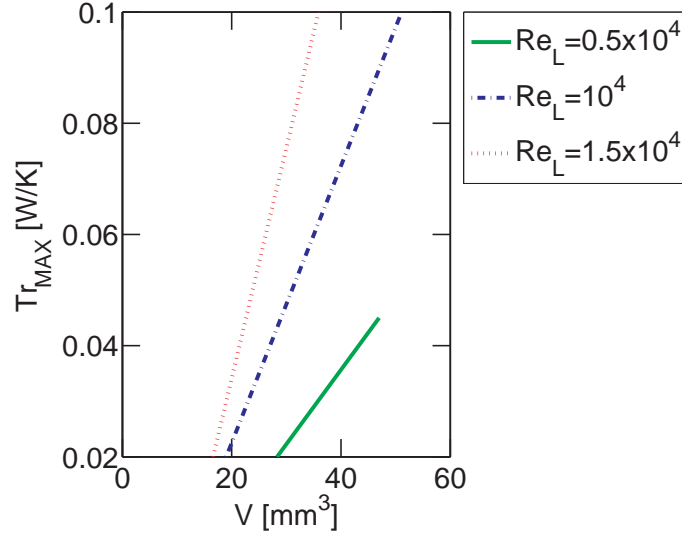
Figure 11: Case study results: Optimal thermal transmittance versus DPP volume.

Table 4: Optimal design parameters for $0.02 < Tr < 0.045 \; [W/K]$ and $Re_L = 0.5 \times 10^4$.

H	d	p	λ_p	$\frac{A}{A_n}$	$\frac{V}{AY_0}$	Tr	V
$[mm]$	$[mm]$	$[mm]$	$[-]$	$[-]$	$[-]$	$[W/K]$	$[mm^3]$
1.77	0.59	1.64	0.13	2.55	1.79	0.020	28.31
2.03	0.64	1.77	0.13	2.66	1.98	0.026	32.58
2.30	0.64	1.77	0.13	2.87	2.07	0.031	36.83
2.55	0.61	1.69	0.13	3.18	2.07	0.037	40.88
2.81	0.58	1.62	0.13	3.50	2.07	0.042	44.94
2.93	0.61	1.69	0.13	3.50	2.17	0.045	46.98
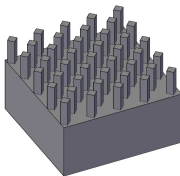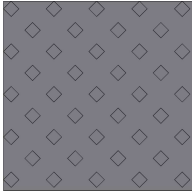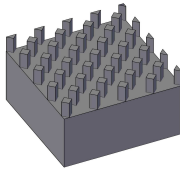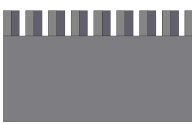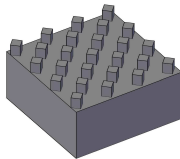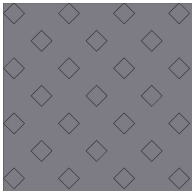
Table 5: Optimal design parameters for $0.02 < Tr < 0.1$ $[W/K]$ and $Re_L = 10^4$.

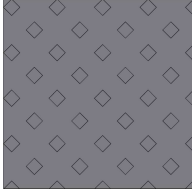| H	d	p	λ_p	$\frac{A}{A_n}$	$\frac{V}{AY_0}$	Tr	V
$[mm]$	$[mm]$	$[mm]$	$[-]$	$[-]$	$[-]$	$[W/K]$	$[mm^3]$
1.18	0.87	2.40	0.13	1.71	1.79	0.020	19.0
1.69	0.61	1.69	0.13	2.45	1.79	0.038	27.1
2.17	0.57	1.58	0.13	2.97	1.88	0.056	34.7
2.55	0.61	1.69	0.13	3.18	2.07	0.073	40.9
2.93	0.61	1.69	0.13	3.50	2.17	0.091	47.0
3.19	0.66	1.84	0.13	3.50	2.35	0.100	51.1

Table 6: Optimal design parameters for $0.02 < Tr < 0.1$ $[W/K]$ and $Re_L = 1.5 \times 10^4$.

H	d	p	λ_p	$\frac{A}{A_n}$	$\frac{V}{AY_0}$	Tr	V
$[mm]$	$[mm]$	$[mm]$	$[-]$	$[-]$	$[-]$	$[W/K]$	$[mm^3]$
0.59	1.08	2.25	0.13	1.50	1.79	0.020	16.6
1.33	0.75	2.08	0.13	1.92	1.79	0.038	21.3
1.62	0.63	1.74	0.13	2.34	1.79	0.056	26.0
1.84	0.58	1.60	0.13	2.66	1.79	0.073	29.5
2.13	0.53	1.48	0.13	3.08	1.79	0.091	34.1
2.24	0.56	1.56	0.13	3.08	1.88	0.100	35.9

Table 7: Optimal design parameters for $Tr = 0.03\ W/K$ at three different Reynolds numbers.

Re_L	Isometric view	Side view	Top view	H	y_0	H/y_0
$[-]$				$[mm]$	$[mm]$	$[-]$
0.5×10^4				2.3	0.076	30
10^4				1.48	0.041	35
1.5×10^4				1.07	0.029	36.5

6. Conclusions

Diamond shaped micro-protruded patterns to enhance convective heat transfer in electronic cooling applications are investigated in this work. Two main goals are achieved:

- The effect of geometrical parameters and fluid dynamic scales on convective heat transfer phenomenon are illustrated.

30

- A methodology suited for the thermal optimization of diamond micro-protruded patterns is proposed and implemented.

Concerning the effect of geometrical parameters and fluid dynamic scales, $Nu_L/Pr^{0.33}$ exhibits a decreasing trend with increasing λ_p. In particular, All DPPs characterized by $\lambda_p > 0.33$ clearly show a heat transfer coefficient lower than the flat case (i.e. no protrusions), due to fluid stagnation. Concerning sparse patterns (low λ_p), it is proved that H plays a key role, namely the dimensionless group $Nu_L/Pr^{0.33}$ monotonically increases with H. In fact, DPP #3, characterized by low λ_p and the highest H among all the tested samples, shows the maximum enhancement in $Nu_L/Pr^{0.33}$ and Tr, up to 150 % and 700 %, respectively. This is due to the fact that high protrusions are able to penetrate deeper in the fluid boundary layer. On the other hand, experimental evidence and optimization procedure suggest the maximum Tr/V, i.e. thermal transmittance per unit of production costs, is reached when $H/y_0 = 30 \div 35$.

A novel methodology is developed for thermal optimization of diamond micro-protruded patterns for heat sinks. An automatic algorithm based on this methodology is implemented and tested. Provided the heat sink working conditions, an optimization procedure is suggested that calculates the optimal geometrical configuration ensuring the required thermal performances while maximizing the thermal transmittance per unit of production costs. Comparing a representative commercial micro-protrusion patterned heat sink with the optimal configuration determined by the algorithm, the second achieves an enhance in thermal performance per unit production cost up to 73% (refer to appendix B for details). This demonstrates that the

proposed methodology may lead to significant improvement in heat transfer performances, while keeping unchanged the production costs.

Finally, it is worth of note that the proposed optimization methodology has rather a general validity, and can be extended to different micro-protruded or micro-structured patterns, especially if manufactured by "not subtractive" techniques. Moreover, this methodology can be easily extended in order to deal with operational costs too (i.e. pressure drops induced by heat sink), by simply substituting η_A to Tr/V as objective function to be maximized.

We expect this work will pave the way to a methodological shift in designing effective heat sinks.

Acknowledgment

Appendix A: Data regression procedure

In the following, the details of data regression presented in Section 4 are exposed. Being $\{\frac{\Delta Tr_R}{V}\}$ the (9×1) column vector whose i-th component is the value of $\frac{\Delta Tr_R}{V}$ of the i-th sample, we impose:

$$\left\{\frac{\Delta Tr_R}{V}\right\} = [M]\{C\}, \tag{18}$$

where $[M]$ is a (9×9) matrix and $\{C\}$ is the (9×1) column vector of model constants defined in Section 4. Being $\{M_i\}$, the i-th row of $[M]$, defined as:

$$\{M_i\} = \left\{ \left(\widehat{\lambda}_p\right)_i, \left(\widehat{\frac{A}{A_n}}\right)_i, \left(\widehat{\frac{V}{AY_0}}\right)_i, \left(\widehat{\lambda_p^2}\right)_i, \left(\widehat{\frac{A}{A_n}}^2\right)_i, \left(\widehat{\frac{V}{AY_0}}^2\right)_i, \right.$$
$$\left. \left(\widehat{\lambda}_p\right)_i \left(\widehat{\frac{A}{A_n}}\right)_i, \left(\widehat{\lambda}_p\right)_i \left(\widehat{\frac{V}{AY_0}}\right)_i, \left(\widehat{\frac{A}{A_n}}\right)_i \left(\widehat{\frac{V}{AY_0}}\right)_i \right\}. \tag{19}$$

$\{M_i\}$ is a vector containing all the geometrical features of the i-th sample. Being $[M]$ and $\left\{\frac{\Delta Tr_R}{V}\right\}$ known, a vector $\{C\}$ containing the unknown constants of the model could be obtained as:

$$\{C\} = [M]^{-1} \left\{\frac{\Delta Tr_R}{V}\right\}, \tag{20}$$

where $[M]^{-1}$ is the inverse of the $[M]$ matrix.

Appendix B: Commercial versus optimized heat sinks

In the following, we compare a representative commercial micro-protrusion patterned (micro pin-fin) heat sink with the optimized patterns presented in section 5.2. In particular, the model 662-15 by Wakefield-vette™ extruded heat sink for integrated circuits is chosen as representative commercial heat sink.

Protrusion base edge $d_c = 1.52\ mm$, protrusion height $H_c = 2.4\ mm$, root surface area $A_{n,c} = (43.5)^2\ mm^2 = 1892\ mm^2$, and number of protrusions $N_c = 168$ of the commercial heat sink are extracted from heat sink data sheet [35]. Protrusions volume is calculated as $V_c = d_c^2 H_c N_c = 931.6\ mm^3$. Moreover, data sheet [35] reports that 662-15 commercial heat sink experiences, for air velocity $u = 965\ LFM = 4.9\ m/s$, a thermal resistance of

2.2 K/W, corresponding to a thermal transmittance $Tr_c = 0.45\ W/K$. The corresponding performance-to-cost ratio is $Tr_c/V_c = 4.88\ 10^{-4}\ W/K/mm^3$.

Values of Tr for the optimized patterns presented in section 5.2 are referred to the root surface area $A_n = 123\ mm^2$. Volume of a 662-15 commercial heat sink characterized by root surface area $= 123\ mm^2$ is $V_c' = VA_n/A_{n,c} = 60.6\ mm^3$, and its transmittance can be estimated as $Tr_c' = Tr_cA_n/A_{n,c} = 0.03\ W/K$. Moreover, fin efficiency of commercial heat sinks (made of aluminum) is nearly 100 % (the same that would be experienced by a copper micro-pin fin heat sink).

Air velocity $u = 4.9\ m/s$ corresponds to a Reynolds number $Re_L = 0.5$ 10^{-4}. Hence 662-15 commercial heat sink will be compared to the optimized heat sink that guarantees $Tr_{opt} = Tr_c' = 0.03\ W/K$ at $Re_L = 0.5\ 10^{-4}$. Drawings and design parameters of this optimized heat sink can be found in 1st row of Tab. 7, and 3rd row of Tab. 4, respectively. Volume of optimal heat sink is $V_{opt} = 36.8\ mm^3$, while the corresponding performance-to-cost ratio is $Tr_{opt}/V_{opt} = 8.42\ 10^{-4}\ W/K/mm^3$.

In conclusion, optimization procedure based on the proposed model leads to enhance Tr/V, i.e. thermal performance per unit production cost, up to 73%, with regard to the considered commercial heat sink.

References

[1] G.E. Moore, Cramming More Components Onto Integrated Circuits, Proceedings of the IEEE 86:1 (1998) 82-85.

[2] S. Gururatana, Heat Transfer Augmentation for Electronic Cooling, American Journal of Applied Sciences 59:1-2 (2012) 436-439.

[3] F. Brighenti, N. Kamaruzaman and J. J. Brandner, Investigation of self-similar heat sinks for liquid cooled electronics, Applied Thermal Engineering 59:1-2 (2013) 725732.

[4] T. Dobre, O. C. Parvulescu, A. Stoica and G. Iavorschi, Characterization of cooling systems based on heat pipe principle to control operation temperature of high-tech electronic components, Applied Thermal Engineering 30:16 (2010) 24352441.

[5] T. Saenen and M. Baelmans, Size effects of a portable two-phase electronics cooling loop, Applied Thermal Engineering 50:1 (2013) 11741185.

[6] S.V. Garimella, A.S. Fleischer, J.Y. Murthy, A. Keshavarzi, R. Prasher, C. Patel, S.H. Bhavnani, R. Venkatasubramanian, R. Mahajan, Y. Joshi, B. Sammakia, B.A. Myers, L. Chorosinski, M. Baelmans, P. Sathyamurthy and P.E. Raad, Thermal Challenges in Next-Generation Electronic Systems, IEEE Transactions on Components and Packaging Technologies 31:4 (2008) 801-815.

[7] V.A.F. Costa and A.M.G. Lopes, Improved radial heat sink for led lamp cooling, Applied Thermal Engineering 70:1 (2014) 131138.

[8] P.A. Deshmukh and R.M. Warkhedkar, Thermal performance of elliptical pin fin heat sink under combined natural and forced convection, Experimental Thermal and Fluid Science 50:61-68 (2013).

[9] W. Yuan, J. Zhao, C.P. Tso, T. Wu, W. Liu and T. Ming, Numerical simulation of the thermal hydraulic performance of a plate pin fin heat sink, Applied Thermal Engineering 48 (2012) 81-88.

35

[10] S. Mancin, C. Zilio, A. Diani, L. Rossetto, Air forced convection through metal foams: Experimental results and modeling, International Journal of Heat and Mass Transfer 62:1 (2013) 112-123.

[11] P.M. Ligrani, G.I. Mahmood, J.L. Harrison, C.M. Clayton, D.L. Nelson, Flow structure and local Nusselt number variations in a channel with dimples and protrusions on opposite walls, International Journal of Heat and Mass Transfer 44:23 (2001) 4413-4425.

[12] M.A. Elyyan, A. Rozati, D.K. Tafti, Investigation of dimpled fins for heat transfer enhancement in compact heat exchangers, International Journal of Heat and Mass Transfer 51:11-12 (2008) 2950-2966.

[13] Y. Chen, Y.T. Chew, B.C. Khoo, Enhancement of heat transfer in turbulent channel flow over dimpled surface, International Journal of Heat and Mass Transfer 55:25-26 (2012) 8100-8121.

[14] K.K. Bodla, S.V. Garimella, J.Y. Murthy, 3D reconstruction and design of porous media from thin sections, International Journal of Heat and Mass Transfer 73 (2014) 250264.

[15] C. Wang, Y. Yu, T. Simon, T. Cui and M.T. North, Microfabrication of short pin fins on heat sink surfaces to augment heat transfer performance, Proceedings of 13th InterSociety Conference on Thermal and Thermomechanical Phenomena in Electronic Systems - ITherm, San Diego (2012).

[16] H. Shafeie, O. Abouali, K. Jafarpur and G. Ahmadi, Numerical study of

heat transfer performance of single-phase heat sinks with micro pin-fin structures, Applied Thermal Engineering 58:1-2 (2013) 68-76.

[17] S.W. Chang, T.-M. Liou, M.H. Lu, Heat transfer of rectangular narrow channel with two opposite scale-roughened walls, International Journal of Heat and Mass Transfer 48:19-20 (2005) 3921-3931.

[18] F. Zhou, and I. Catton, Obtaining closure for a plane fin heat sink with elliptic scale-roughened surfaces for Volume Averaging Theory (VAT) based modeling, International Journal of Thermal Sciences 71 (2013) 264-273.

[19] M. I. Shahzad, M. Giorcelli, L. Ventola, D. Perrone, N. Shahzad, E. Chiavazzo, P. Asinari, M. Cocuzza and A. Tagliaferro, Convective Heat Transfer Enhancement for Electronic Device Applications using Patterned MWCNTs Structures, Heat Transfer Engineering (2015), DOI:10.1080/01457632.2015.1080570.

[20] L. Ventola, E. Chiavazzo, F. Calignano, D. Manfredi and P. Asinari, Heat Transfer Enhancement by Finned Heat Sinks with Microstructured Roughness, Journal of Physics: Conference Series 494 (2014) 012009.

[21] L. Ventola, F. Robotti, M. Dialameh, F. Calignano, D. Manfredi, E. Chiavazzo and P. Asinari, Rough surfaces with enhanced heat transfer for electronics cooling by direct metal laser sintering, International Journal of Heat and Mass Transfer 75 (2014) 58-74.

[22] L. Ventola, L. Scaltrito, S. Ferrero, G. Maccioni, E. Chiavazzo and P. Asinari, Micro-structured rough surfaces by laser etching for heat transfer enhancement on flush mounted heat sinks, Journal of Physics: Conference Series 525 (2014) 012017.

[23] E. Chiavazzo, L. Ventola, F. Calignano, D. Manfredi, P. Asinari, A sensor for direct measurement of small convective heat fluxes: Validation and application to micro-structured surfaces, Experimental Thermal and Fluid Science 55 (2014) 42-53.

[24] S.V. Garimella and P.A. Eibeck, Heat transfer characteristics of an array of protruding elements in single phase forced convection, Internal Journal of Heat and Mass Transfer 33:12 (1990) 2659-2669.

[25] C.W. Leung, H.J. Kang, S.D. Probert, Horizontal simulated printed-circuit board assembly in fully-developed laminar-flow convection, Applied Energy 56 (1997) 71-91.

[26] C.S.B. Grimmond, T.R. Oke, Aerodynamic Properties of Urban Areas Derived from Analysis of Surface, Form. J. Appl. Meteor. 38 (1999) 1262-1292.

[27] S.B. Pope, Turbulent Flows, Cambridge University Press, 2000.

[28] R. L. Mason, R. F. Gunst and J. L. Hess, Statistical Design and Analysis of Experiments: With Applications to Engineering and Science, 2nd ed., John Wiley, Hoboken (2003).

[29] H. Schlichting, K. Gersten, Boundary-layer theory, Springer, 8th ed., Berlin, 2000.

[30] D.E. Maddox and I. Mudawar, Single- and two-phase convective heat transfer from smooth and enhanced microelectronic heat sources in a rectangular channel, Journal of Heat Transfer 111:4 (1989) 1045-1052.

[31] C.P. Tso, G.P. Xu, K.W. Tou, An Experimental Study on Forced Convection Heat Transfer From Flush-Mounted Discrete Heat Sources, Journal of Heat Transfer 121 (1999) 326-332.

[32] A. Bejan and A.D. Kraus (Editors), Heat Transfer Handbook, John Wiley, Hoboken (2003).

[33] S.C. Jenkins, B. Weigand, J. von Wolfersdorf, S.O. Neumann, Validation and Analysis of Numerical Results for a Varying Aspect Ratio Two-Pass Internal Cooling Channel, Journal of Heat Transfer 133 (2011) 051701.

[34] C.T. Chen and H.I. Chen, Multi-objective optimization design of plate-fin heat sinks using a direction-based genetic algorithm, Journal of the Taiwan Institute of Chemical Engineers, 44 (2013) 257265.

[35] http://www.wakefield-vette.com/resource-center/downloads/brochures/intergrated-heatsink-wakefield.pdf